

Trimmed Sampling Algorithm for the Noisy Generalized Eigenvalue Problem

Caleb Hicks¹ and Dean Lee¹

¹Facility for Rare Isotope Beams and Department of Physics and Astronomy, Michigan State University, MI 48824, USA

The generalized eigenvalue problem is an efficient technique for finding extremal eigenvalues and eigenvectors of large quantum systems. It uses subspace projection to define Hamiltonian and norm matrices corresponding to some set of non-orthogonal states. Unfortunately the method often involves the inversion of norm matrices that are ill-conditioned and therefore highly susceptible to noise. This is especially problematic when matrix elements are evaluated using stochastic methods and have substantial error bars. In this work we introduce the trimmed sampling algorithm, which is able to substantially reduce the effects of noise. Using the framework of Bayesian inference, we sample prior probability distributions for the Hamiltonian and norm matrices along with physics-informed constraints about positivity of the norm matrix and convergence of extremal eigenvalues with respect to subspace size. The final output is a probability distribution for the eigenvectors and observables which automatically comes with a reliable estimate of the error and performs far better than standard regularization methods. The method should have immediate use for a wide range of applications from classical to quantum computing.

INTRODUCTION

One common approach for finding extremal eigenvalues and eigenvectors of large quantum systems is to project onto basis states that have good overlap with the eigenvector of interest. Since these states are often not orthogonal to each other, this process results in a generalized eigenvalue problem of the form $H|\psi\rangle = EN|\psi\rangle$, where H is the projected Hamiltonian matrix, N is the norm matrix for the non-orthogonal basis, E is the energy, and $|\psi\rangle$ is the column vector for the projected eigenvector. If O is the projected matrix for some other observable using the same basis, then we can compute expectation values of that observable using $\langle O \rangle = \langle \psi|O|\psi\rangle / \langle \psi|N|\psi\rangle$.

The generator coordinate method is a well-known technique in nuclear physics, where the corresponding generalized eigenvalue problem is called the Hill-Wheeler equation [1–4]. The generalized eigenvalue problem is used in several computational approaches utilizing variational subspace methods and non-orthogonal bases [5–7]. It serves as a cornerstone of methods such as eigenvector continuation [8–13] and the more general class of reduced basis methods [14–16]. It is also useful for Monte Carlo simulations where trial states are produced using Euclidean time projection starting from several different initial and final states [17–21].

By using only a small subspace of states, the generalized eigenvalue problem can, in principle, make very efficient use of computational resources. However, one major weakness is the increased sensitivity to error. One needs to find eigenvectors and eigenvalues of the matrix $N^{-1}H$, and the condition number of the norm matrix grows larger as the size of the subspace grows. In some cases, even very small errors due to the limits of machine precision can cause problems. The problem is most severe when stochastic methods such as Monte Carlo simulations are used to compute the elements of the Hamiltonian and norm matrices, and the resulting uncertainties can be quite substantial. It is also relevant for quantum computing using variational subspace methods, where one must consider both statistical errors as well as

systematic errors due to gate errors, measurement errors, and decoherence [22, 23].

There are well-established methods for dealing with ill-posed inverse problems. Tikhonov regularization is one popular approach [24], and the simplest form of Tikhonov regularization is ridge regression or nugget regularization. In this approach a small positive multiple of the identity, ϵI , is added to the norm matrix that needs to be inverted. However, it is not straightforward to choose an appropriate value for ϵ [25] nor to estimate the systematic bias introduced by the regularization.

In this work we introduce the trimmed sampling algorithm, which uses physics-based constraints and Bayesian inference [26, 27] to reduce errors of the generalized eigenvalue problem. Instead of simply regulating the norm matrix, we sample probability distributions for the Hamiltonian and norm matrix elements weighted by likelihood functions derived from physics-informed constraints about positivity of the norm matrix and convergence of extremal eigenvalues with respect to subspace size. We then determine a posterior distribution for the Hamiltonian and norm matrix elements and sample eigenvectors and observables from that distribution. The method is described in the next section, and then we then apply the trimmed sampling to two challenging benchmark calculations. After this, we analyze the performance and discuss new applications that may be possible based upon this work and its extensions.

METHODS

Let us label the basis states used to define the generalized eigenvalue problem as $|v_1\rangle, |v_2\rangle, \dots, |v_n\rangle, \dots$. As noted above, there is no assumption that the states are orthogonal or normalized. Let us define E_n as the ground state energy for the generalized eigenvalue problem if we truncate after the first n basis states,

$$H^{(n \times n)} |\psi_n\rangle = E_n N^{(n \times n)} |\psi_n\rangle. \quad (1)$$

If the matrix elements of H and N could be determined exactly, then the variational principle tells us that the sequence E_n must be monotonically decreasing and bounded below by the true ground state energy E_{exact} . We will assume that the basis states $|v_1\rangle, |v_2\rangle, \dots |v_n\rangle, \dots$ have been ordered so that the energies E_n converge to E_{exact} as a smoothly-varying function of n for sufficiently large n .

The problem is that we do not have exact calculations of the H and N matrices. Instead start with some estimates for the Hamiltonian and norm matrices, which we call \tilde{H} and \tilde{N} respectively. We also are given one-standard-deviation error estimates for each element of the Hamiltonian and norm matrices, which denote as $\Delta\tilde{H}$ and $\Delta\tilde{N}$ respectively. In this work we consider the standard case where the Hamiltonian and norm matrices are manifestly Hermitian. But we also discuss the generalization to the non-Hermitian case at the end of our analysis.

We will compute a posterior probability distribution $P(H, N|R)$ for the elements of the Hamiltonian matrix H and norm matrix N . Here R indicates a set of physics-informed conditions we impose on the H and N matrices, and the corresponding likelihood function is written as $P(R|H, N)$. We also include a prior probability distribution, which we write as $P(H, N)$. From Bayes' theorem, the posterior distribution is given by

$$P(H, N|R) = \frac{P(R|H, N)P(H, N)}{\int \prod_{ij} [dH_{ij} dN_{ij}] P(R|H, N)P(H, N)}. \quad (2)$$

For our prior distribution, we take a product of uncorrelated Gaussian functions,

$$P(H, N) = \prod_{ij} \frac{e^{-\frac{(H_{ij} - \tilde{H}_{ij})^2}{2(\Delta\tilde{H}_{ij})^2}} e^{-\frac{(N_{ij} - \tilde{N}_{ij})^2}{2(\Delta\tilde{N}_{ij})^2}}}{2\pi\Delta\tilde{H}_{ij}\Delta\tilde{N}_{ij}}, \quad (3)$$

though a more detailed model of the prior distribution with asymmetric errors and correlations among matrix elements can be also implemented.

Our likelihood function $P(R|H, N)$ is a product of two factors,

$$P(R|H, N) = f_{\text{pos}}(N)f_C(H, N). \quad (4)$$

The first factor, $f_{\text{pos}}(N)$, enforces the constraint that the norm matrix must be positive definite. It equals 1 if N is positive definite and equals 0 otherwise. The second factor $f_C(H, N)$ is a function of the submatrix energies E_n given in Eq. (1). Let us define the convergence ratio C_n for $n > 2$ as

$$C_n = \frac{E_n - E_{n-1}}{E_{n-1} - E_{n-2}}. \quad (5)$$

We have taken ratios of energy differences for consecutive energies E_n . This can be generalized to ratios of energy differences between non-consecutive energies in cases where the convergence pattern has some periodicity. Let C_{max} be the maximum of C_n over all n . We define C to be a conservative

upper bound estimate for C_{max} . We then take the second likelihood factor, $f_C(H, N)$, to have the form

$$f_C(H, N) = e^{-\frac{C_{\text{max}}}{C}}. \quad (6)$$

The purpose of this likelihood function is to penalize the likelihood of Hamiltonian and norm matrices whose convergence rate for the ground state energies is much slower than expected and C_{max} is significantly larger than C . Neither the exact value for C nor the exact functional form for $f_C(H, N)$ are essential features that need to be finely tuned. Similar results can be obtained using a wide range of different choices, and for some applications a different definition for $f_C(H, N)$ may prove to be more effective.

In order to sample the posterior distribution in $P(H, N|R)$ in Eq. (2), we first produce random samples for the Hamiltonian and norm matrices using a heat bath algorithm given by the prior probability distribution $P(H, N)$. We then reweight the samples according to the likelihood function $P(R|H, N)$. From this sampling of the posterior distribution, we can compute median values and estimated error bars for energies or any other observable.

BOSE HUBBARD MODEL

For the first benchmark test of the trimmed sampling algorithm, we consider the Bose Hubbard model in three-dimensions. This system describes a system of identical bosons on a three-dimensional lattice, with a Hamiltonian that contains a hopping term proportional to t , a contact interaction proportional to U , and a chemical potential proportional to μ . We will consider the system with four bosons on a $4 \times 4 \times 4$ lattice with $\mu = -6t$. Following the analysis in Ref. [8], we use eigenvector continuation (EC) to determine the ground state energy for a range of couplings U/t . For our basis states we use the ground state eigenvectors for five training values, $U/t = -2.5, -1.9, -1.8, -1.7, -1.6$.

In order to introduce noise into the EC calculations, we round each entry of the H and N matrices at the sixth decimal place and use these rounded values for our estimates \tilde{H} and \tilde{N} . Since the rounding error is performed at the sixth digit, we use the error estimates $\Delta\tilde{H}_{ij} = \Delta\tilde{N}_{ij} = \frac{1}{\sqrt{12}} \times 10^{-6}$. For our n^{th} order EC calculation, we use the first n basis states and apply trimmed sampling.

The results for the ground state energies E_0/t versus coupling U/t are shown in Fig. 2 for orders $n = 4, 5$. The “exact” ground state energies are shown with solid lines. The “noiseless EC” results are shown with dashed lines. The “noisy EC” results corresponding with matrix elements \tilde{H} and \tilde{N} are shown with open circles. The results obtained using “ridge regression” are shown with times symbols. We have tried to optimize the parameter ϵ used in ridge regression to produce the best possible performance. The “raw data” obtained by sampling the prior probability distribution $P(H, N)$ associated with \tilde{H} and \tilde{N}

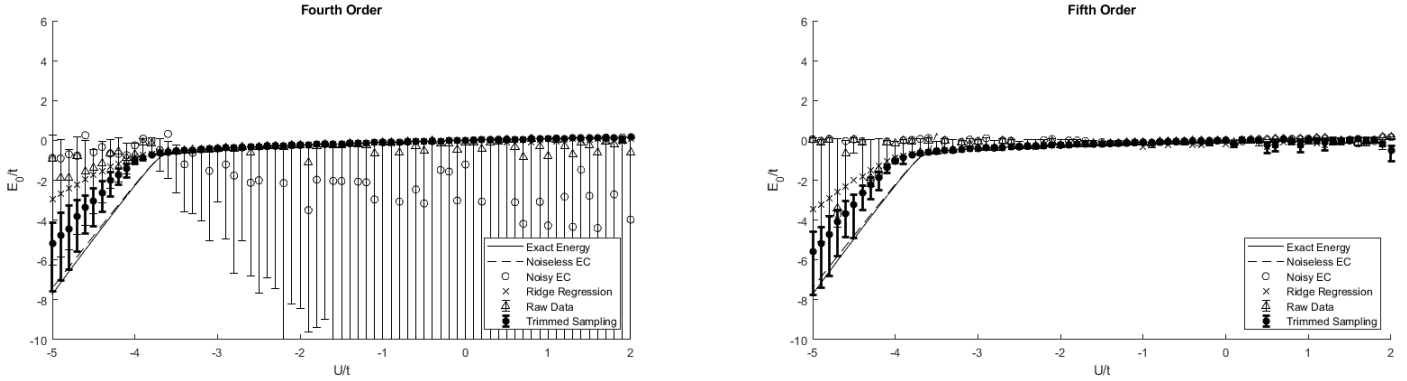


FIG. 1. Ground state energy of the Bose Hubbard model as a function of coupling strength U/t . The “exact” ground state energies are plotted as solid lines. The “noiseless EC” data are shown with dashed lines. The “noisy EC” results corresponding with matrix elements \tilde{H} and \tilde{N} are shown with open circles. The results using “ridge regression” are shown with times symbols. The “raw data” obtained by sampling the prior probability distribution are shown with open triangles and error bars. The “trimmed sampling” results are plotted as filled circles with error bars.

and uncertainties $\Delta\tilde{H}$ and $\Delta\tilde{N}$ are shown with open triangles and error bars.

The “trimmed sampling” results are obtained by sampling the posterior probability distribution $P(H, N|R)$ and plotted as filled circles with error bars. For all of our plots showing error bars, the plot symbol is located at the weighted median value while the lower and upper limits correspond to the 16th and 84th percentiles respectively. We find that this representation of the error bars is useful since the distributions have much heavier tails than Gaussian distributions. For all of the trimmed sampling results present here, we have produced 500 samples with nonzero posterior probability, and the small matrix calculations can be performed easily on a single processor.

We use the value $C = 2.5$ for $f_C(H, N)$ in Eq. (6). The trimmed sampling algorithm is clearly doing a good job of controlling errors due to noise. There is some systematic underestimation of the error near the avoided level crossing at $U/t = -3.8$. But away from the avoided level crossing, the overall error estimate is fairly accurate in predicting the agreement with noiseless EC results. The trimmed sampling algorithm is performing significantly better than the standard regularization provided by ridge regression.

HEISENBERG MODEL

For the second benchmark test, we consider a one-dimensional quantum Heisenberg chain. The Hamiltonian for this system is

$$H_J = -J \sum_{j=1}^N [\sigma_j^x \sigma_{j+1}^x + \sigma_j^y \sigma_{j+1}^y + \sigma_j^z \sigma_{j+1}^z] \quad (7)$$

Here $\sigma^x, \sigma^y, \sigma^z$ are the Pauli matrices, N is the number of sites, and J is the coupling. We consider the case with $N = 10$ sites and calculate the lowest four energy eigenvalues of

the subspace with $\sum_j \sigma_j^z = 0$. For more details of the model, see Ref. [28].

For the generalized eigenvalue problem, we construct our basis states using Euclidean time projection, starting from the initial state $|v_0\rangle = |01010101\rangle$. We operate on $|v_0\rangle$ with the Euclidean time projection operator, e^{-Ht} . We consider values of J ranging from 0.5 to 1.5. For each value of J , we take the Euclidean time values $t_n = 0.1n$ and define each basis vector as $|v_n\rangle = e^{-Ht_n} |v_0\rangle$ for $n = 0, 1, 2, 3, 4, 5$. After projecting onto these six vectors, we calculate the corresponding Hamiltonian and norm matrices and solve the generalized eigenvalue problem.

In order to introduce noise into the calculation, we apply random Gaussian noise with standard deviation $\sigma = 0.01$ to each element of the Hamiltonian and norm matrices. These resulting matrices with noise included define our estimates \tilde{H} and \tilde{N} , and we take the uncertainty estimates to be $\Delta\tilde{H}_{ij} = \Delta\tilde{N}_{ij} = 0.01$. For each value of J , the observables we compute are the lowest four energy eigenvalues. Since J is just an overall scale for the Hamiltonian, the exact energies will just scale linearly with J . However, the Euclidean time projection calculations will be quite different for each J due to the fixed projection times t_n used. The effects of the random noise will vary with J .

The results are shown in Fig. 2. The “exact” energies calculated using exact diagonalization are shown with solid lines. The “noiseless time projection” results are shown with dashed lines. The “noisy time projection” results corresponding with matrix elements \tilde{H} and \tilde{N} are shown with open circles. The results obtained using “ridge regression” are shown with times symbols. We have tried to optimize the parameter ϵ used in ridge regression to produce the best possible performance, though the overall improvement is not significant. The “raw data” obtained by sampling the prior probability distribution $P(H, N)$ associated with mean values \tilde{H} and \tilde{N} and uncertainties $\Delta\tilde{H}$ and $\Delta\tilde{N}$ are shown with open

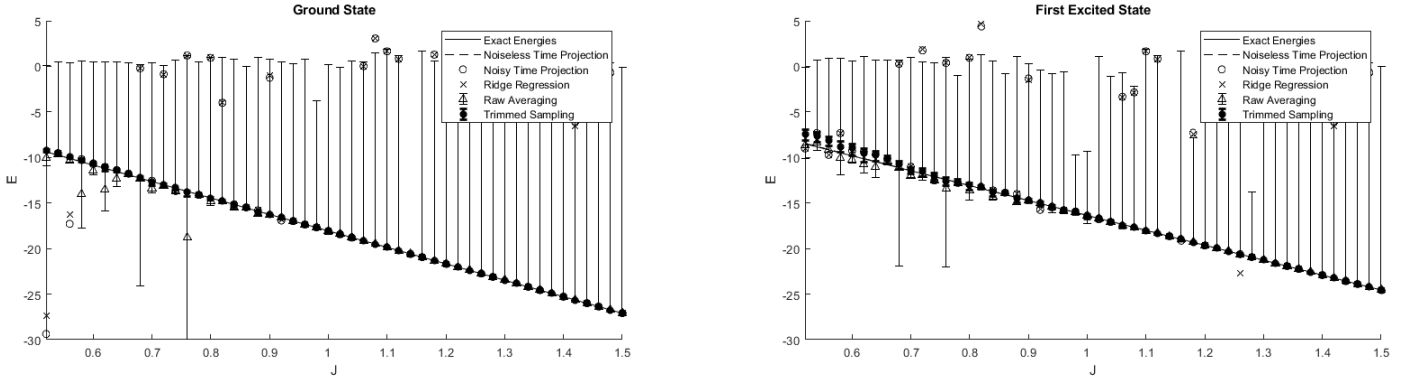


FIG. 2. Ground state and first excited state energies of the one-dimensional Heisenberg chain as a function of coupling strength J . The “exact” energies are plotted as solid lines. The “noiseless time projection” data are dashed lines. The “noisy time projection” results corresponding with matrix elements \hat{H} and \hat{N} are shown with open circles. The data obtained using “ridge regression” are shown with times symbols. The “raw data” obtained by sampling the prior probability distribution are shown with open triangles and error bars. The “trimmed sampling” results are plotted as filled circles with error bars.

triangles and error bars.

The “trimmed sampling” results are obtained by sampling the posterior probability distribution $P(H, N|R)$ and plotted as filled circles with error bars. These results use the value $C = 2.5$ for $f_C(H, N)$ in Eq. (6). The trimmed sampling algorithm is again doing a good job of controlling errors due to noise, and the error estimate is fairly accurate in predicting the agreement with “noiseless time projection” results. In contrast, ridge regression is not giving consistently reliable results for this benchmark test.

In addition to calculating energies for the Heisenberg model, we can also compute spin observables. In Fig. 3 we show results for the ground-state expectation value of the product of nearest-neighbor spins $\langle \sigma_1^z \sigma_2^z \rangle$ in the left panel and the product of next-to-nearest-neighbor spins $\langle \sigma_1^z \sigma_3^z \rangle$ in the right panel. The trimmed sampling algorithm is again performing significantly better than ridge regression. The error estimate is also fairly accurate in estimating the agreement with “noiseless time projection” results.

DISCUSSION AND OUTLOOK

The generalized eigenvalue problem is a useful method for finding the extremal eigenvalues and eigenvectors of large quantum systems. However, the approach is highly susceptible to noise. We have presented the trimmed sampling algorithm, which uses the framework of Bayes inference to incorporate information about the prior probability distribution for the Hamiltonian and norm matrix elements together with physics-informed likelihood constraints. The result is a posterior probability distribution that can easily be sampled. For the benchmark examples presented here, we find that trimmed sampling performs significantly better than standard regularization methods such as ridge regression. We have demonstrated significant error reductions for energy

calculations as well as other observables. In the Supplemental Material, we present several other additional benchmark calculations that further demonstrate the performance of the trimmed sampling algorithm.

The trimmed sampling algorithm can be used for any generalized eigenvalue problem obtained using classical computing or quantum computing. This encompasses a very wide class of problems ranging from quantum many body systems to partial differential equations to quantum field theories. All that is needed are some good estimates for the Hamiltonian and norm matrix elements and their corresponding uncertainties. In order to gain the full advantage of the trimmed sampling algorithm, it is important that matrix calculations are performed using machine precision that is finer than the uncertainties of the Hamiltonian and norm matrix elements. Studies of the trimmed sampling algorithm for the non-Hermitian Hamiltonian and norm matrices are currently under investigation. In that case one cannot simply impose positivity of the norm matrix in the likelihood function. However, one can instead impose more stringent conditions on the convergence of the energies E_n for the submatrix calculations.

Acknowledgements We are grateful for discussions with Joey Bonitati, Serdar Elhatisari, Gabriel Given, Zhengrong Qian, Avik Sarkar, Jacob Watkins, and Xilin Zhang. We acknowledge financial support from the U.S. Department of Energy (DE-SC0021152 and DE-SC0013365) and the NUCLEI SciDAC-4 collaboration.

- [1] D. L. Hill and J. A. Wheeler, Phys. Rev. **89**, 1102 (1953).
- [2] J. J. Griffin and J. A. Wheeler, Phys. Rev. **108**, 311 (1957).
- [3] C. Wa Wong, Physics Reports **15**, 283 (1975), ISSN 0370-1573.
- [4] P. Magierski, P. H. Heenen, and W. Nazarewicz, Phys. Rev. C **51**, R2880 (1995), nucl-th/9503001.

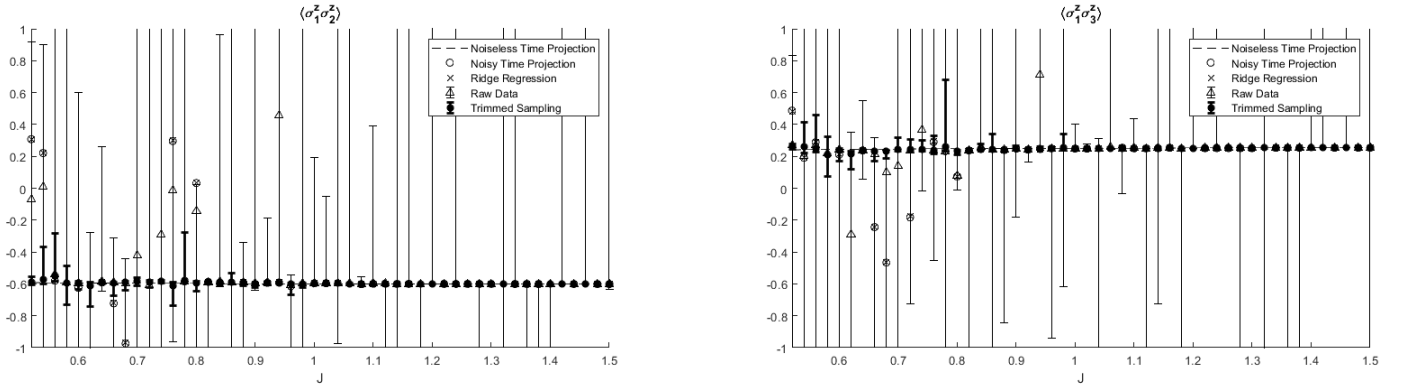


FIG. 3. Spin pair expectation values for the ground state of the Heisenberg model as a function of J . $\langle \sigma_1^z \sigma_2^z \rangle$ is shown in the left panel and $\langle \sigma_1^z \sigma_3^z \rangle$ is shown in the right panel. The plot symbols are the same as in Fig. 2.

- [5] K. Varga and Y. Suzuki, Phys. Rev. C **52**, 2885 (1995), nucl-th/9508023.
- [6] D. Blume and K. M. Daily, Phys. Rev. A **80**, 053626 (2009), 0909.2701.
- [7] T. Togashi, Y. Tsunoda, T. Otsuka, N. Shimizu, and M. Honma, Phys. Rev. Lett. **121**, 062501 (2018), 1806.10432.
- [8] D. Frame, R. He, I. Ipsen, D. Lee, D. Lee, and E. Rrapaj, Phys. Rev. Lett. **121**, 032501 (2018), 1711.07090.
- [9] P. Demol, T. Duguet, A. Ekström, M. Frosini, K. Hebeler, S. König, D. Lee, A. Schwenk, V. Somà, and A. Tichai, Phys. Rev. C **101**, 041302 (2020), 1911.12578.
- [10] S. König, A. Ekström, K. Hebeler, D. Lee, and A. Schwenk, Phys. Lett. B **810**, 135814 (2020), 1909.08446.
- [11] A. Ekström and G. Hagen, Phys. Rev. Lett. **123**, 252501 (2019), 1910.02922.
- [12] R. J. Furnstahl, A. J. Garcia, P. J. Millican, and X. Zhang, Phys. Lett. B **809**, 135719 (2020), 2007.03635.
- [13] A. Sarkar and D. Lee, Phys. Rev. Lett. **126**, 032501 (2021), 2004.07651.
- [14] A. Quarteroni, A. Manzoni, and F. Negri, *Reduced Basis Methods for Partial Differential Equations: An Introduction*, vol. 92 (Springer, 2015).
- [15] E. Bonilla, P. Giuliani, K. Godbey, and D. Lee (2022), 2203.05284.
- [16] J. A. Melendez, C. Drischler, R. J. Furnstahl, A. J. Garcia, and X. Zhang (2022), 2203.05528.
- [17] L. Liu, G. Moir, M. Pardon, S. M. Ryan, C. E. Thomas, P. Vilaseca, J. J. Dudek, R. G. Edwards, B. Joo, and D. G. Richards (Hadron Spectrum), JHEP **07**, 126 (2012), 1204.5425.
- [18] R. G. Edwards, N. Mathur, D. G. Richards, and S. J. Wallace (Hadron Spectrum), Phys. Rev. D **87**, 054506 (2013), 1212.5236.
- [19] S. Elhatisari, The European Physical Journal A **55** (2019), ISSN 1434-601X.
- [20] S. Shen, T. A. Lähde, D. Lee, and U.-G. Meißner, Eur. Phys. J. A **57**, 276 (2021), 2106.04834.
- [21] S. Shen, T. A. Lähde, D. Lee, and U.-G. Meißner (2022), 2202.13596.
- [22] A. Peruzzo, J. McClean, P. Shadbolt, M.-H. Yung, X.-Q. Zhou, P. J. Love, A. Aspuru-Guzik, and J. L. O'Brien, Nature Communications **5**, 4213 (2014), 1304.3061.
- [23] E. F. Dumitrescu, A. J. McCaskey, G. Hagen, G. R. Jansen, T. D. Morris, T. Papenbrock, R. C. Pouser, D. J. Dean, and P. Lougovski, Phys. Rev. Lett. **120**, 210501 (2018), 1801.03897.
- [24] A. N. Tikhonov, Doklady Akademii Nauk SSSR **39**, 195 (1943).
- [25] M. Naif, International Journal of statistics & economics 0975-556x **7**, 10 (2011).
- [26] A. Gelman, J. Carlin, H. Stern, and D. Rubin, *Bayesian Data Analysis* (Chapman and Hall/CRC, 1995).
- [27] D. R. Phillips et al., J. Phys. G **48**, 072001 (2021), 2012.07704.
- [28] K. Choi, D. Lee, J. Bonitati, Z. Qian, and J. Watkins, Phys. Rev. Lett. **127**, 040505 (2021).

SUPPLEMENTAL MATERIALS

Additional benchmark calculations

We present some additional benchmark calculations of the trimmed sampling algorithm using the one-dimensional quantum Heisenberg chain presented in the main text. As described there, we construct basis states using Euclidean time projection, starting from the initial state $|v_0\rangle = |0101010101\rangle$. We operate on $|v_0\rangle$ with the Euclidean time projection operator, e^{-Ht} . For each value of J , we take the Euclidean time values $t_n = 0.1n$ and define each basis vector as $|v_n\rangle = e^{-Ht_n}|v_0\rangle$ for $n = 0, 1, 2, 3, 4, 5$. After projecting onto these six vectors, we calculate corresponding the Hamiltonian and norm matrices and solve the generalized eigenvalue problem. In order to introduce noise into the calculation, we apply random Gaussian noise with standard deviation $\sigma = 0.01$ to each element of the Hamiltonian and norm matrices.

In Fig. S1, we show results for the energies of the second excited state and third excited state of the Heisenberg model. The “exact” energies calculated using exact diagonalization are shown with solid lines. The “noiseless time projection” results are shown with dashed lines. The “noisy time projection” results corresponding with matrix elements \tilde{H} and \tilde{N} are shown with open circles. The results obtained using “ridge regression” are shown with times symbols. We have tried to optimize the parameter ϵ used in ridge regression to produce the best possible performance, though the overall improvement is not significant. The “raw data” obtained by sampling the prior probability distribution $P(H, N)$ associated with mean values \tilde{H} and \tilde{N} and uncertainties $\Delta\tilde{H}$ and $\Delta\tilde{N}$ are shown with open triangles and error bars. The “trimmed sampling” results are plotted as filled circles with error bars. These results use the value $C = 2.5$ for $f_C(H, N)$. We see that the trimmed sampling algorithm is performing significantly better than ridge regression. The error estimate is fairly accurate in estimating the agreement with “noiseless time projection” results.

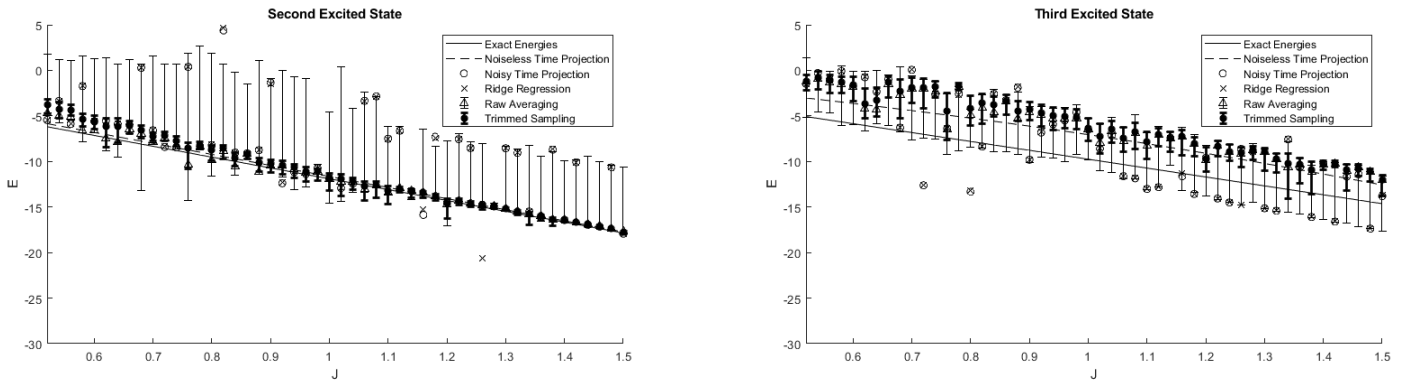


FIG. S1. Second and third excited state energies of the one-dimensional Heisenberg chain as a function of coupling strength J . The “exact” energies are plotted as solid lines. The “noiseless time projection” data are dashed lines. The “noisy time projection” results corresponding with matrix elements \tilde{H} and \tilde{N} are shown with open circles. The data obtained using “ridge regression” are shown with times symbols. The “raw data” obtained by sampling the prior probability distribution are shown with open triangles and error bars. The “trimmed sampling” results are plotted as filled circles with error bars.

In Fig. S2 we show results for spin pair expectation values for the first excited state of the Heisenberg model. The product of nearest-neighbor spins $\langle\sigma_1^z\sigma_2^z\rangle$ is shown in the left panel, and the product of next-to-nearest-neighbor spins $\langle\sigma_1^z\sigma_3^z\rangle$ is shown in the right panel. These results use the value $C = 2.5$ for $f_C(H, N)$. The trimmed sampling algorithm is once again performing better than ridge regression. The error estimate is fairly accurate in estimating the agreement with “noiseless time projection” results.

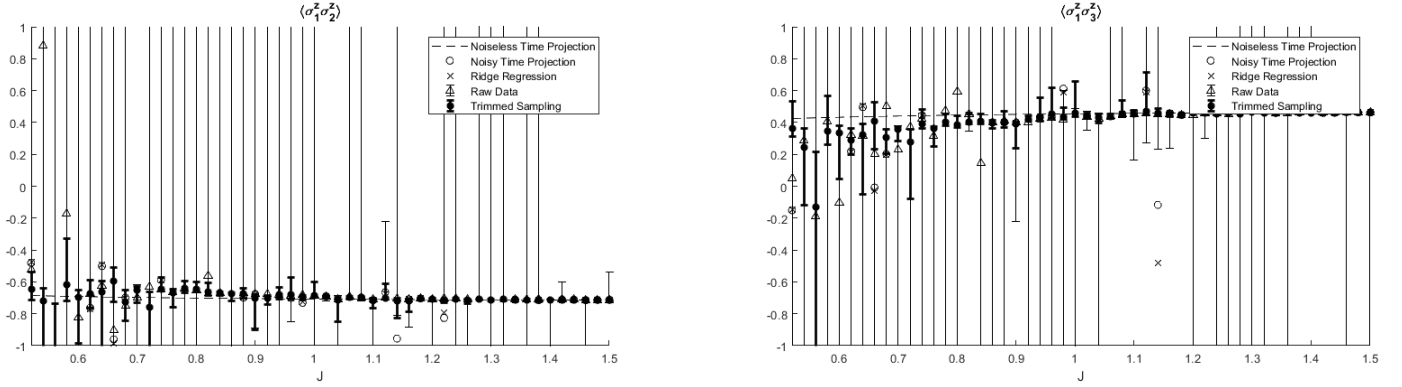


FIG. S2. Spin pair expectation values for the first excited state of the Heisenberg model as a function of J . $\langle \sigma_1^z \sigma_2^z \rangle$ is shown in the left panel and $\langle \sigma_1^z \sigma_3^z \rangle$ is shown in the right panel. The plot symbols are the same as in Fig. S1.